On the effects on cortical spontaneous activity of the symmetries of the network of pinwheels in visual area V1.

Romain Veltz, Pascal Chossat, Olivier Faugeras

On the effects on cortical spontaneous activity of the symmetries of the network of pinwheels in visual area V1.

Romain Veltz, Pascal Chossat, Olivier Faugeras

RESEARCH REPORT
N° 01079055
Octobre 2014
Project-Team NeuroMathComp

ISSN 0249-6399 ISRN INRIA/RR--01079055--FR+ENG

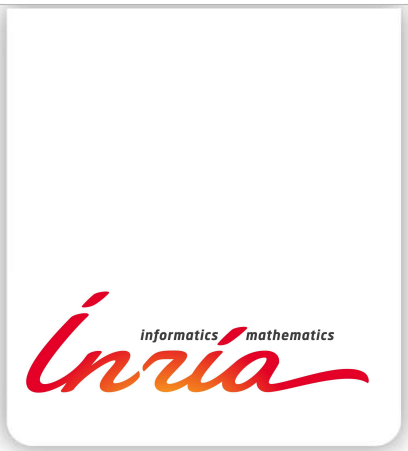

On the effects on cortical spontaneous activity of the symmetries of the network of pinwheels in visual area V1.

Romain Veltz*, Pascal Chossat†, Olivier Faugeras ‡

Project-Team NeuroMathComp

Research Report n° 01079055 — Octobre 2014 — 29 pages

This work was partially supported by the European Union Seventh Framework Programme (FP7/2007-2013) under grant agreement no. 269921 (BrainScaleS), no. 318723 (Mathemacs), and by the ERC advanced grant NerVi no. 227747.

* NeuroMathComp team.
† CNRS and NeuroMathComp team.
‡ NeuroMathComp team.

RESEARCH CENTRE
SOPHIA ANTIPOLIS – MÉDITERRANÉE

2004 route des Lucioles - BP 93
06902 Sophia Antipolis Cedex

Abstract: This paper challenges and significantly extends the seminal work in [EC79, BCG+01]. We consider the problem of describing mathematically the spontaneous activity of V1 by combining several important experimental observations including 1) the organization of the visual cortex into a spatially periodic network of hypercolumns structured around pinwheels, 2) the difference between short-range and long-range intra-cortical connections, the first ones being rather isotropic and producing naturally doubly-periodic patterns by Turing mechanisms, the second one being patchy and 3) the fact that the Turing patterns spontaneously produced by the short-range connections and the network of pinwheels have similar periods. By analyzing the Preferred Orientation (PO) map, we are able to classify all possible singular points of the PO maps (the pinwheels) as having symmetries described by a small subset of the wallpaper groups. We then propose a description of the spontaneous activity of V1 using a classical voltage-based neural field model that features isotropic short-range connectivities modulated by non-isotropic long-range connectivities. A key observation is that, with only short-range connections and because the problem has full translational invariance in this case, a spontaneous doubly-periodic pattern generates a 2-torus in a suitable functional space which persists as a flow-invariant manifold under small perturbations, hence when turning on the long-range connections. Through a complete analysis of the symmetries of the resulting neural field equation and motivated by a numerical investigation of the bifurcations of their solutions, we conclude that the branches of solutions which are stable over an extended set of parameters are those corresponding to patterns with an hexagonal (or nearly hexagonal) symmetry. The question of which patterns persist when turning on the long-range connections is answered by 1) analyzing the remaining symmetries on the perturbed torus and 2) combining this information with the Poincaré-Hopf theorem. We have developed a numerical implementation of the theory that has allowed us to produce the patterns of activities predicted by the theory, the planforms. In particular we generalize the contoured and non-contoured planforms predicted by previous authors [EC79, BCG+01] and predict the existence of mixed contoured/non-contoured planforms. We also found that these planforms are most likely to be time evolving.

Key-words: No keywords

Effets des symmétries du réseau de pinwheels de l'aire corticale visuelle V1 sur l'activité corticale spontanée.

Résumé : Pas de résumé

Mots-clés : Pas de motclef

1 Introduction

The primary area (V1) of the visual cortex is one of the first locations targeted by connections from the Thalamus which relay (and process) inputs from the retina. In some mammals like primates, cats or ferrets (see [HW62, HW77, KSL+10]), this cortical area is very precisely organized in modules, called cortical hypercolumns, which process visual attributes (like local orientation, spatial frequency) of different points in the visual field. Note that there is almost no experimental evidence of hypercolumns from histology (see [LAB03a]). Most of our knowledge derives from functional evidence, *i.e.* when an external stimulus is applied. In this work, we focus on the processing of the local orientation of visual stimuli which is reflected by the ability of some neurons to fire only when a drifting grating of specific (called preferred) orientation is presented in their receptive field. The distribution, on the cortical sheet, of the preferred orientation of these particular neurons (see [BS86, GLF+86]) defines a *Preferred Orientation map* (hereafter called the PO map) which has a near lattice structure and which is continuous except at particular points called pinwheels.

It has been argued by several authors (Ermentrout [EC79], Bressloff and Cowan [BCG+01, BC02]), that V1 is to some extent structured like a crystal: it can be approximated by a plane where the pinwheels are arranged in a doubly-periodic lattice and the main features of cortical activity in V1 can be interpreted in this framework. This idealization naturally introduces symmetries in the problem, which make deeper analysis accessible. As long as the pinwheels are nearly arranged on a periodic lattice we can expect that the main conclusions of our analysis will be still valid for the "real" lattice.

There is also experimental evidence (see below) that the spatial distribution of connections emanating from one neuron in V1 differs according to whether the connections are *local* (within one hypercolumn) or *long-range* (between different hypercolumns). Local connections are considered to be isotropic. In the absence of long-range connections the network (or field) of local connections would be Euclidian-invariant, that is invariant under rigid displacements and reflections in the plane, a property that is transmitted to the model equations [EC79]. On the other hand, long-range connections are subject to the constraint of respecting the symmetries of the OP map, thereby reducing the full Euclidean group symmetries to a crystallographic subgroup associated with the lattice of pinwheels. Moreover experimental observations suggest that the strength of long-range connections is significantly weaker than that of local connections, which allows for treating the long-range connections as a perturbation of the local ones.

However as shown initially by Ermentrout and Cowan [EC79], spontaneous activity of V1 without long-range connections also produces naturally doubly-periodic steady patterns by Turing mechanism [Tur52]. This fact has been at the origin of a series of papers where hallucinatory patterns (seen by patients under the influence of drugs or other stimuli of the visual cortex which are not coming from the Thalamus) have been explained as Turing patterns bifurcating in V1 [BCG+01, GST03]. It was assumed in these papers that the lattice of pinwheels can be itself approximated as a continuum in the plane, that is, every point in the plane is a pinwheel. Then the full system of connections, local and long-range, keeps translation invariance: any planar translation applied to a pattern yields another one, up to periodicity. Therefore a pattern is not an isolated solution but rather generates a manifold of solutions under the action of translations, which is called an *orbit* under the action of the group of translations. This orbit, thanks to the periodicity of the pattern, can be identified with a 2-torus in a suitable functional space. Moreover as long as this torus is a *normally hyperbolic* manifold (it means here that steady-state patterns are hyperbolic along directions transversal to the orbit), it persists as a flow-invariant manifold under small perturbations.

When the lattice of pinwheels is discrete, long-range connections reduce the translation group

$\mathbb{R}^2$ to a discrete subgroup isomorphic to $\mathbb{Z}^2$. Our aim in this paper is to study the effect of switching on such long-range connections on the tori of solutions of the system with local connections only. As in the above cited papers we assume that the strength of long-range connections is small compared to that of local connections. The introduction of the long-range connections destroys part of the symmetries but not all of them. The perturbed torus possesses these remaining symmetries. We classify possible dynamics on this invariant manifold by applying topological methods (Poincaré-Hopf theorem) together with the symmetries. Numerical (direct) simulations of the equations then allow to determine which phase portrait is actually observed among those which have been theoretically identified.
Our motivation for this work is to understand how introducing a discrete lattice of pinwheels would modify the states and dynamics of spontaneous activity in V1, and we expect this could have some consequences on the theory of hallucinations of Bressloff, Golubitsky et al. in [BCG+01].

The problem of the effect of long-range connections with discrete translation invariance, on the Turing patterns which bifurcate when these connections are inactive, has been addressed by Bressloff [Bre03] (see also Cowan and Baker [BC09]) in the following context. These authors assumed that the periods of the patterns and of the lattice of pinwheels were not correlated. An analysis inspired by methods initially introduced for hydrodynamical systems allowed them to build Ginzburg-Landau equations, in order to describe the slow modulation of the bifurcating patterns under the effect of periodic forcing due to the long-range connections.

There are however some experimental observations which suggest that in fact, due to synaptic plasticity, the periods of the pinwheel lattice and of the Turing patterns are close to each other [KBT+03, MSL+05]. It is therefore not unrealistic to assume that these periods are in fact equal, which we do in this study. Our approach differs on another point: we do not assume the system to be close to bifurcation from homogeneous state. Therefore the validity range of our results goes well beyond bifurcation analysis, and also it allows for a rigorous mathematical treatment in the spirit of Lauterbach and Roberts [LR92] about forced symmetry breaking of group orbits of equilibria with spherical symmetry.

The way by which neurons in V1 acquire orientation selectivity is still controversial as the connections from the Thalamus provide a very small percentage of the inputs: 95% of these inputs are made of recurrent connections, i.e. intracortical connections (see [DKM+95]). Despite this experimental evidence there are still two extreme attitudes to account for these facts: either we assume that the recurrent connections provide much of the input to each neuron, or that each neuron mostly follows the thalamic input, discarding the recurrent connections, see [FPF07]. Our approach lies in-between.

We use the following standard neural field representation for the neural activity V of the neuron located at $\mathbf{x}$ in the connected domain Ω of $\mathbb{R}^2$ representing V1:

$$\frac{d}{dt}V(\mathbf{x},t) = -V(\mathbf{x},t) + \int_\Omega J(\mathbf{x},\mathbf{y})\mathbf{S}(V(\mathbf{y},t))d\mathbf{y} + I_{thalamus}(\mathbf{x},t). \tag{1}$$

The domain Ω is usually taken as the infinite plane. This is not an unrealistic approximation in the analysis because the number of pinwheels in V1 is rather large, typically several thousands [BCG+01]. However in numerical computations one has to choose a bounded domain and the simplest choice is a square with periodic boundary conditions: opposite sides are identified.

The connectivity function J represents the intracortical connections between neurons and $I_{thalamus}$ the thalamic input. $\mathbf{S}$ is an increasing function with range $(0,1)$, typically sigmoidal, with slope σ at the origin. Following [Bre03], we decompose the connectivity function as follows:

$$J(\mathbf{x},\mathbf{y}) = J_{loc}(\mathbf{x},\mathbf{y}) + \epsilon_{LR}J_{LR}(\mathbf{x},\mathbf{y}), \quad \epsilon_{LR} << 1 \tag{2}$$

where J_{loc} models the local connections and $J_{LR}(\mathbf{x},\mathbf{y})$ models the long-range connections. The small factor ϵ_{LR} in front of J_{LR} accounts for the fact mentioned above that the strength of the long-range connections is significantly weaker than that of the short-range connections [HG91]. From [LAB03b, MSL+05] we can assume that the local connections are isotropic (rotation invariant), and we further assume for simplicity that they are also homogeneous (translation invariant). Hence J_{loc} only depends on the distance between $\mathbf{x}$ and $\mathbf{y}$:

$$J_{loc}(\mathbf{x},\mathbf{y}) = J_{loc}(\|\mathbf{x}-\mathbf{y}\|).$$

$\|\mathbf{x}-\mathbf{y}\|$ is the usual Euclidean norm in $\mathbb{R}^2$. The form of the function J_{LR} is discussed in Section 3.1. The external (thalamic) input function $I_{thalamus}$ will be assumed equal to 0 throughout the paper in order to consider spontaneous activity only.

Let us have a look at the bifurcation diagram in Figure (1). It shows bifurcated patterns in a square Ω with periodic boundary conditions when only local connections are involved. The bifurcation parameter in abscissa is the slope of the sigmoid function $\mathbf{S}$. It shows as expected two primary bifurcated branches: one of stripes and one of "spots", which correspond to a periodic pattern with square symmetry. Near bifurcation other types of solutions branch off these primary branches. Observe that the stripes are always unstable and that the spots are stable in a small interval, up to the first secondary bifurcation. On the other hand two secondary branches of doubly periodic states bifurcate sub-critically and recover stability after bending back in the increasing σ direction. These states are then stable on large intervals of values of σ. In their stability domain they look pretty much like hexagonal patterns. In fact they approximate the exact hexagonal patterns that would bifurcate on a domain with hexagonal symmetry (and periodic boundary conditions). If the size of Ω is increased, these two branches come closer from each other and bifurcate closer from the primary bifurcation point. In the limit of a domain with infinite size, they merge into one branch which bifurcates at the same point as the spots and stripes and they correspond exactly to the hexagonal patterns which are well-known from Turing theory of pattern formation.
Since we are interested in stable states, we can consider in the analysis, instead of these "imperfect hexagons", the exact hexagonal patterns that will show up in an hexagonal lattice. This will make the analysis simpler and richer at the same time, and the results will still be relevant for the secondary "approximate" hexagonal patterns observed in Fig. (1). Despite the fact that square patterns (spots in Fig 1) are stable only in a small region near bifurcation, we shall discuss both square and hexagonal patterns for completeness.

Our primary motivation here is to understand how the long-range connections with discrete lattice symmetry affect the dynamics of the network. This is made possible by using the fact that these connections act as a perturbation [HG91] of the dynamics generated by the local connections. Looking at the spontaneous activity, *i.e.* without thalamic input, is motivated by two reasons. The first reason is that it has been argued that the hallucinating patterns generated by some drugs can be explained by the spontaneous activity of networks [EC79, BCG+01] similar to the one studied here. The second reason is that if we were to include an input with amplitude ϵ that we vary, it would be the same as working with a fixed amplitude but varying the slope of the sigmoid function $\mathbf{S}$ [VF10]. Hence, looking at the case of a thalamic input can be thought as a deformation of the case considered here.

The paper is organized as follows.
PLAN.

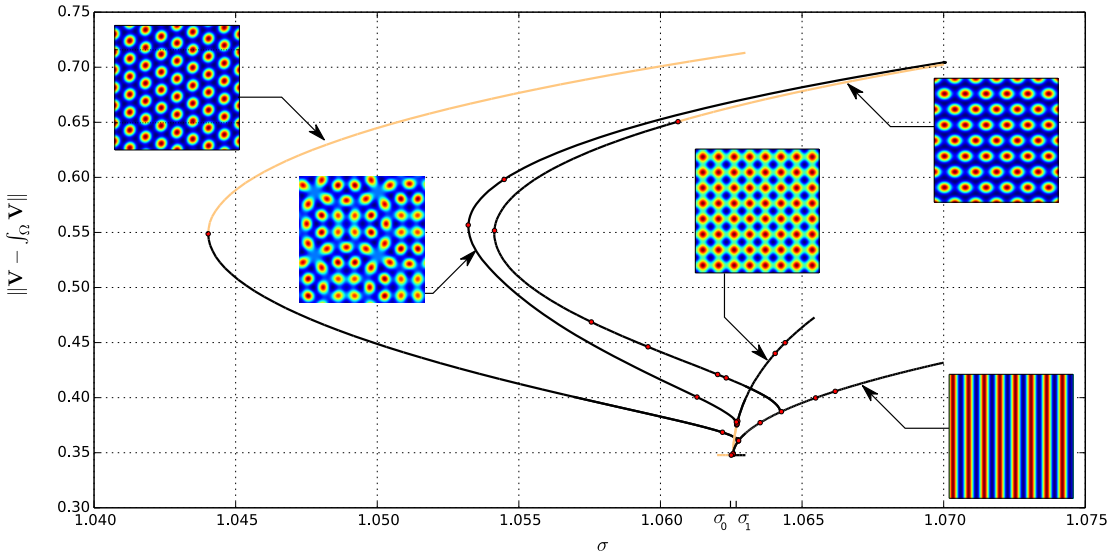

Figure 1: Incomplete bifurcation diagram of (1) w.r.t. the slope parameter σ, when $I_{thalamus} = 0$ and $J(\mathbf{x}, \mathbf{y})$ is a difference of gaussians on a square domain with periodic boundary conditions. Black lines correspond to unstable solutions and brown to stable solutions. Each non constant solution yields a torus of solutions because of the boundary conditions. The red dots are bifurcation points. The connectivity is tuned such that the first bifurcation point for the nonlinear gain σ is a supercritical $\mathbf{D}_4$-pitchfork bifurcation with wave-vector $\|\mathbf{k}\| = 1$ for which the spots are stable and the stripes not. Note how this bifurcation diagram is similar to the $\mathbf{D}_6$-pitchfork case. The size of the square cortex is $8 \times 2\pi$ and the number of unknowns is 1024^2.

2 Turing patterns in the unperturbed case

In this section, we formulate our assumptions on the symmetries of the unperturbed solutions[1], written $V_0(\mathbf{x})$, that will be analyzed upon switching on the long-range connections. The computation of Turing patterns has been extensively documented in the literature (see for example [Hoy06] for a review and [EC79] for neural fields), we will no cover it but briefly recall the main results. We have seen in the introduction that when $\epsilon_{LR} = 0$, the system is invariant under any translation in the periodic domain Ω. Adjusting Ω to be a square or an hexagon, branches of steady patterns with square or hexagonal symmetry bifurcate from the homogeneous state as the slope σ of the sigmoid function S reaches a threshold value. These patterns are stable in some range of values of σ as shown in Fig. 1. Stability here means "orbital stability". Indeed any translation applied to such a state V_0 gives another pattern of the system thanks to the translational invariance. The group of translations acting in Ω (which has periodic boundaries) is the torus $\mathbb{R}^2/\mathbb{Z}^2$, which moreover acts faithfully on any V_0 with square or hexagonal pattern. Therefore the set (called *translation group orbit*) of translated states from V_0 is a torus manifold. Moreover this torus is an attractor if V_0 is orbitally stable.

A central hypothesis of the current study is the assumption that the spatial period of $\mathbf{V}_0$ matches the spatial period of the PO map. The experimental data that supports this assumption was already mentioned in the introduction. The approximate 'hexagonal' patterns (in the square cortex as in Figure 1) does not satisfy our assumption. Also, the stripes[2] patterns will not be studied here. Indeed, in these cases the patterns have less symmetries and their study would require minor modifications of the present argument.

3 Network symmetries

A central assumption in our analysis is that the pinwheels are organized as a lattice which has the same periodic structure as the patterns which bifurcate when long-range connections are off. For reasons which have been explained in the introduction we are interested in the perturbation of Turing patterns with square or hexagonal symmetries. Such patterns have maximal lattice symmetry, meaning that they are invariant under the dihedral group of rotations/reflections $\mathbf{D}_k$ with $k = 4$ (squares) or 6 (hexagons), and of course they are invariant under discrete translations which define the lattice group. It is therefore convenient to suppose that the domain Ω representing the primary visual cortex is a square or a hexagon with periodic boundary conditions (opposite sides are identified). Let $\mathbf{e}_1$, $\mathbf{e}_2$ be two vectors generating the lattice and Ω_0 be a fundamental domain centered at the origin O of Ω (see Figure 2). We choose $\mathbf{e}_1$ and $\mathbf{e}_2$ as unit vectors and making an angle of $\pi/2$ in the square case, $\pi/3$ in the hexagonal case. Then

$$\Omega_0 = \left\{ O + x_1\mathbf{e}_1 + x_2\mathbf{e}_2 \mid -\frac{\ell}{2} \leq x_i < \frac{\ell}{2},\ i = 1, 2 \right\},$$

and by construction there exists an integer N such that, by periodicity,

$$\Omega \simeq \{\Omega_0 + j_1\mathbf{e}_1 + j_2\mathbf{e}_2 \mid j_1, j_2 = -N, \dots, N\}.$$

There are $(2N+1)^2$ copies of Ω_0 in Ω. Choosing a suitable length scale we further assume that $\ell = 2\pi$. The number N will be adjusted to match the number of elementary cells produced in Ω by the bifurcation of patterns when only local connections are active.

[1] in effect doubly-periodic solutions
[2] which satisfy our assumption

Let us now describe how pinwheels are distributed in Ω. Pinwheels are the singular points of the OP map at which no orientation is preferred. Together with the orientation map they introduce an anisotropy in the lattice, reducing the symmetry group $\mathbf{D}_k \ltimes \mathbb{Z}^2_{2N}$ of the lattice in Ω to a *crystallographic* subgroup (see [Cox61, Mil72, Sch78] for an introduction), which is called, in the two-dimensional, case a *wallpaper group*,[3]. It is well-known that there are 17 such groups, up to isomorphism. However there are restrictions on the number of possible patterns of pinwheels. First, we only consider square and hexagonal lattices. Second, in order to be biologically plausible the patterns built from the orientation map must be continuous except at pinwheels. We have determined by inspection that over all possibilities, only those displayed in Fig. 2 are compatible with these constraints. Pinwheels are the points (black/white dots in the pictures) at which all colors meet. Each color in Fig. 2 defines an orientation, which we identify with an angle between $-\pi/2$ and $\pi/2$.

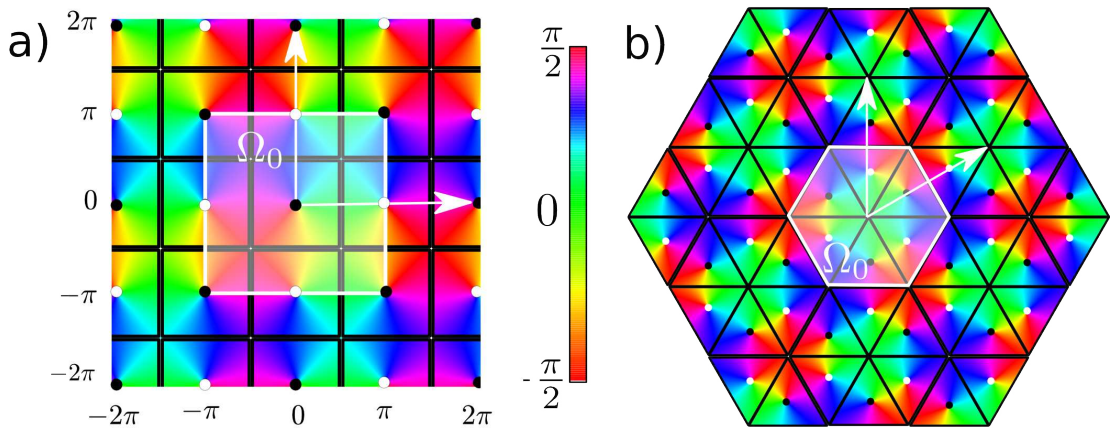

Figure 2: The two pinwheel lattices considered in this work in the square case (a) and in the hexagonal case (b). The black lines show the elementary domains (the hypercolumns), the white lines the fundamental domains Ω_0 (see text). The clockwise (resp. counterclockwise) pinwheels are represented with black (resp. white) dots. The vectors $2\pi\mathbf{e}_1$ and $2\pi\mathbf{e}_2$ are shown in white.

Remark 1 We centered the hypercolumns around the pinwheels and used a uniform preferred orientation density such that the proportion of neurons coding for each orientation is the same for each orientation. This is done in order to avoid any preference of the network for a particular orientation. Note that pinwheels come by pairs called counterclockwise and clockwise: at a counterclockwise (respectively clockwise) pinwheel, the orientation map shows increasing orientations when turning counterclockwise (respectively clockwise) around it. Finally notice that the fundamental domain is either centered at a pinwheel (Fig. 2.a), or not (Fig. 2.b).

To be rigorous the set of orientations should be identified with the projective line $P^1(\mathbb{R})$. We can further identify $P^1(\mathbb{R})$ with the interval $\left(-\frac{\pi}{2}, \frac{\pi}{2}\right]$. Let $\mathcal{P}$ be the set of pinwheels in Ω, then the OP map is a map

$$\theta : \Omega \setminus \mathcal{P} \to \left(-\frac{\pi}{2}, \frac{\pi}{2}\right].$$

Note that $P^1(\mathbb{R})$ is diffeomorphic to the circle $S^1 \simeq (-\pi, \pi]$ *mod* 2π through the map $\left(-\frac{\pi}{2}, \frac{\pi}{2}\right] \ni \varphi \mapsto 2\varphi$. This allows to naturally define an action of the circle group S^1 on $P^1(\mathbb{R})$: if $\mathbf{R}_\phi$ is the

[3]In fact in our problem it would be suitable to use the notion of *color group* [].

rotation of angle $\phi \in S^1$ around the origin, then $\mathbf{R}_\phi(\varphi) = \varphi + h(\phi)/2$ where h is a homomorphism of S^1. From there, we can define an action of S^1 on the map θ as follows. Let $\phi_0 = \pi/2$ in the square case and $\phi_0 = 2\pi/3$ in the hexagonal case and let $\mathbf{R}^{\mathbf{p}}_\phi$ be the rotation of angle ϕ centered on a pinwheel $\mathbf{p}$. Then, with the OP maps of Fig. 2,

$$\theta(\mathbf{R}^{\mathbf{p}}_{\phi_0}\mathbf{x}) = \theta(\mathbf{x}) + \epsilon\frac{\phi_0}{2} \tag{3}$$

where $\epsilon = 1$ if the pinwheel is counterclockwise and -1 otherwise.
Similarly, let $\mathbf{K}$ be the reflection w.r.t. to a line passing through a pinwheel and parallel to the vector $\mathbf{e}_1$ (horizontal axis). For the OP maps of Fig. 2,

$$\theta(\mathbf{K}\mathbf{x}) = -\theta(\mathbf{x}). \tag{4}$$

This defines an action of the reflection $\mathbf{K}$ on the map θ. In order to transfer these relations as (possible) symmetries of the network, we use the action of $\mathbf{D}_k \ltimes \mathbb{Z}^2_{2N}$ on $\mathrm{L}^2(\Omega, \mathbb{R})$:

$$(\gamma, V) \to \left(\mathbf{x} \to \gamma \cdot V(\mathbf{x}) = V(\gamma^{-1}\mathbf{x})\right).$$

This allows to write (3) as $(\mathbf{R}^{\mathbf{p}}_{\phi_0})^{-1} \cdot \theta = \theta + \epsilon\frac{\phi_0}{2}$.

Remark 2 Note that the value of the orientation map could well be shifted by some arbitrary $\theta_0 \in \left(-\frac{\pi}{2}, \frac{\pi}{2}\right]$ *while keeping its quality of being an orientation map. Except when* $\theta_0 = 0$ *or* $\pm\pi/2$*, this would have the effect of breaking the reflection symmetry of* θ *because applying the new reflection would not preserve the lattice. In the case of the tree shrew, the cortical coordinates (here assumed to be equal to visual field coordinates) must be such that the zero level of the OP map is parallel to the* x_1*-axis. In this case, the reflection* $\mathbf{K}$ *acts indeed on the network. On the other hand, for the macaque, any value of* θ_0 *is relevant. Hence in this case this assumption is somewhat artificial. Nevertheless the presence of a reflection symmetry has strong consequences on the dynamics and we shall subsequently consider both the reflection and non reflection cases.*

Let us first draw a consequence of the relation (3) that will play a major role in the following analysis.

Lemma 3.1 *Let* $\alpha\mathbf{e}_1$, $\alpha > 0$*, be the vector between two closest pinwheels of different types in the direction* $\mathbf{e}_1$*.* α *is the smallest distance between them. Then (3) implies that:*

$$\mathbf{T}_{\mathbf{t}} \cdot \theta(\mathbf{x}) = \theta(\mathbf{x} - \mathbf{t}) = \theta(\mathbf{x}) + \phi_0, \quad \mathbf{t} = \alpha(\mathbf{e}_1 + \mathbf{e}_2). \tag{5}$$

Proof. Let us write $\mathbf{R}^{\mathbf{p}_{cc}}_{\phi_0}$ (resp. $\mathbf{R}^{\mathbf{p}_c}_{\phi_0}$) the rotation of angle ϕ_0 around a counterclockwise (resp. clockwise) pinwheel. According to (3) we have $(\mathbf{R}^{\mathbf{p}_{cc}}_{\phi_0})^{-1} \cdot \mathbf{R}^{\mathbf{p}_c}_{\phi_0} \cdot \theta = \theta + \phi_0$. From Lemma A.1 $(\mathbf{R}^{\mathbf{p}_{cc}}_{\phi_0})^{-1}\mathbf{R}^{\mathbf{p}_c}_{\phi_0}\mathbf{x} = \mathbf{x} + \mathbf{t}$ with $\mathbf{t} = ((\mathbf{R}^{\mathbf{o}}_{\phi_0})^{-1} - Id)(-\alpha\mathbf{e}_1)$. This gives $\mathbf{t} = \alpha(\mathbf{e}_1 + \mathbf{e}_2)$ and $\mathbf{T}_{\mathbf{t}} \cdot \theta = \theta + \phi_0$.

We have $\alpha = \pi$ in the square case and $\alpha = 2\pi/3$ in the hexagonal case (cf. Figure 2).

3.1 Model and symmetries of the long-range connections

In macaques, the anisotropy of horizontal connections follows from the anisotropy of the visual field representation in V1, *i.e.* it is not correlated to a feature like orientation [ALW+02]: the patchiness of the connections is hence isotropic. There are at least two ways to take this fact into account in the mathematical model of the long-range connections. The first was introduced initially by Bressloff [Bre03]:

$$J^{bressloff}_{LR}(\mathbf{x}, \mathbf{y}) = G_{\sigma_\theta}\left(\theta(\mathbf{x} - \mathbf{y})\right) J_0(\chi, \mathbf{R}^{\mathbf{o}}_{2\theta(\mathbf{x})}(\mathbf{x} - \mathbf{y})) \tag{6}$$

where $J_0(\chi,\mathbf{x}) = e^{-\left[(1-\chi)^2x_1^2+x_2^2\right]/2\sigma_{LR}^2}$. When $\chi = 0$ the connectivity is isotropic while when $\chi = 1$ is "the most" anisotropic. By the form of the first factor, we see that it produces homogeneous patchy connections. The second way differs mainly[4] by precisely this first factor which is replaced by $G_{\sigma_\theta}(\theta(\mathbf{x})-\theta(\mathbf{y}))$.

$$J_{LR}(\mathbf{x},\mathbf{y}) = G_{\sigma_\theta}\left(\theta(\mathbf{x})-\theta(\mathbf{y})\right)J_0(\chi,\mathbf{R}^{\mathbf{o}}_{-2\theta(\mathbf{x})}\left(\mathbf{x}-\mathbf{y}\right)). \tag{7}$$

It was introduced by [Vel11] because the expression $\theta(\mathbf{x}-\mathbf{y})$ is somewhat artificial. Note that the use of (7) instead is more natural but it destroys the homogeneity of the long-range connections featured by (6). This is the model which we consider in this article.

We now turn to the examination of the invariance properties of the long-range connections with respect to the symmetries of the network of pinwheels and orientation map. The function J_{LR} is invariant under a transformation $\gamma \in \mathbf{D}_k \ltimes \mathbb{Z}^2_{2N}$ if $J_{LR}(\gamma\mathbf{x},\gamma\mathbf{y}) = J_{LR}(\mathbf{x},\mathbf{y})$ for all $\mathbf{x},\mathbf{y}$. This implies that the equations are equivariant with respect to the action defined in the previous section for the transformation γ. We consider successively the cases of square and hexagonal lattices. However there are some general features which are shared by both types of networks and we start by stating them.

Lemma 3.2 *We have* $J_{LR}(\mathbf{R}^{\mathbf{p}_{cc}}_{\phi_0}\mathbf{x},\mathbf{R}^{\mathbf{p}_{cc}}_{\phi_0}\mathbf{y}) = J_{LR}(\mathbf{x},\mathbf{y})$

Proof. From (3), the factor $G_{\sigma_\theta}\left(\theta(\mathbf{x})-\theta(\mathbf{y})\right)$ is clearly unaffected by the rotations. Now thanks to (3) and the expression $\mathbf{R}^{\mathbf{p}_{cc}}_{\phi_0}\mathbf{x} = \mathbf{R}^{\mathbf{o}}_{\phi_0}(\mathbf{x}-\mathbf{p}_{cc})+\mathbf{p}_{cc}$,

$$\begin{aligned} J_0\left(\chi,\mathbf{R}^{\mathbf{o}}_{-2\theta(\mathbf{R}^{\mathbf{p}_{cc}}_{\phi_0}\mathbf{x})}(\mathbf{R}^{\mathbf{p}_{cc}}_{\phi_0}\mathbf{x}-\mathbf{R}^{\mathbf{p}_{cc}}_{\phi_0}\mathbf{y})\right) &\overset{(3)}{=} J_0\left(\chi,\mathbf{R}^{\mathbf{o}}_{-2\theta(\mathbf{x})-\phi_0}(\mathbf{R}^{\mathbf{p}_{cc}}_{\phi_0}\mathbf{x}-\mathbf{R}^{\mathbf{p}_{cc}}_{\phi_0}\mathbf{y})\right)\\ &= J_0\left(\chi,\mathbf{R}^{\mathbf{o}}_{-2\theta(\mathbf{x})-\phi_0}\mathbf{R}^{\mathbf{o}}_{\phi_0}(\mathbf{x}-\mathbf{y})\right)\\ &= J_0\left(\chi,\mathbf{R}^{\mathbf{o}}_{-2\theta(\mathbf{x})}(\mathbf{x}-\mathbf{y})\right). \end{aligned}$$

Note that in the square case, the above result still holds for $\epsilon = -1$ because $2\phi = \pi$ in this case and J_0 is an even function.

Lemma 3.3 *Let* $\mathbf{K}$ *be the reflection across the horizontal axis. Assume that (4) holds. Then* $J_{LR}(\mathbf{K}\mathbf{x},\mathbf{K}\mathbf{y}) = J_{LR}(\mathbf{x},\mathbf{y})$.

Proof. The factor $G_{\sigma_\theta}\left(\theta(\mathbf{x})-\theta(\mathbf{y})\right)$ is clearly unaffected by the reflection. Now thanks to (4),

$$\begin{aligned} J_0\left(\chi,\mathbf{R}^{\mathbf{o}}_{-2\theta(\mathbf{K}\mathbf{x})}\mathbf{K}(\mathbf{x}-\mathbf{y})\right) &= J_0\left(\chi,\mathbf{R}^{\mathbf{o}}_{2\theta(\mathbf{x})}\mathbf{K}(\mathbf{x}-\mathbf{y})\right)\\ &= J_0\left(\chi,\mathbf{K}\mathbf{R}^{\mathbf{o}}_{-2\theta(\mathbf{x})}(\mathbf{x}-\mathbf{y})\right) = J_0\left(\chi,\mathbf{R}^{\mathbf{o}}_{-2\theta(\mathbf{x})}(\mathbf{x}-\mathbf{y})\right). \end{aligned}$$

Lemma 3.4 *Let* $\mathbf{t}$ *be the vector as in Lemma 3.1. Let* $\gamma = \mathbf{T}^{-1}_{\mathbf{t}}\mathbf{R}^{\mathbf{p}_c}_{\phi_0}$. *Then* $J_{LR}(\gamma\mathbf{x},\gamma\mathbf{y}) = J_{LR}(\mathbf{x},\mathbf{y})$.

Proof. We can rewrite Lemma 3.1 as $\mathbf{T}^{-1}_{\mathbf{t}}\cdot\theta = \theta-\phi_0$. Hence, we have $\gamma\cdot\theta = \theta-\frac{\phi_0}{2}$. We now look at the effect on the long-range connections. The factor $G_{\sigma_\theta}\left(\theta(\mathbf{x})-\theta(\mathbf{y})\right)$ is clearly

[4] Note also the difference with (6) for the rotation term. The main reason is to implement co-circularity [Vel11].

unaffected by the transformation γ. Now, thanks to the previous relation:

$$\begin{aligned} J_0\left(\chi, \mathbf{R}^{\mathbf{o}}_{-2\theta(\gamma^{-1}\mathbf{x})}(\gamma^{-1}\mathbf{x}-\gamma^{-1}\mathbf{y})\right) &= J_0\left(\chi, \mathbf{R}^{\mathbf{o}}_{-2\theta(\gamma^{-1}\mathbf{x})}((\mathbf{R}^{\mathbf{p}_c}_{\phi_0})^{-1}\mathbf{x}-(\mathbf{R}^{\mathbf{p}_c}_{\phi_0})^{-1}\mathbf{y})\right) \\ &= J_0\left(\chi, \mathbf{R}^{\mathbf{o}}_{-2\theta(\gamma^{-1}\mathbf{x})}(\mathbf{R}^{\mathbf{p}_c}_{-\phi_0}\mathbf{x}-\mathbf{R}^{\mathbf{p}_c}_{-\phi_0}\mathbf{y})\right) \\ &= J_0\left(\chi, \mathbf{R}^{\mathbf{o}}_{-2\theta(\gamma^{-1}\mathbf{x})}\mathbf{R}^{\mathbf{o}}_{-\phi_0}(\mathbf{x}-\mathbf{y})\right) \\ &= J_0\left(\chi, \mathbf{R}^{\mathbf{o}}_{-2(\theta(\mathbf{x})-\phi_0/2)-\phi_0}(\mathbf{x}-\mathbf{y})\right) \\ &= J_0\left(\chi, \mathbf{R}^{\mathbf{o}}_{-2\theta(\mathbf{x})}(\mathbf{x}-\mathbf{y})\right). \end{aligned}$$

Applying γ to the previous equation gives the γ invariance.

We will now use these lemmas to derive the generators of the symmetry group in the square and hexagonal cases. We will also compute the specific crystallographic group that they generate.

3.1.1 The square case

We are now in position to derive the symmetry group of the network equations. Note that the case of the Bressloff connectivity (6) leads to a different symmetry group. We start with the generators.

Proposition 3.5 *We write $\mathbf{R}^{\mathbf{p}_c}_{\phi_0}$ the rotation of angle $\frac{\pi}{2}$ centered on a clockwise pinwheel. For the (PMM) PO map in Figure 2 a, the symmetry group associated with the connectivity (7) in the case $\chi > 0, \epsilon_{LR} \neq 0$ is:*

1. $\Gamma = \left\langle \mathbf{K}, \mathbf{R}^{\mathbf{p}_c}_{\phi_0}, \mathbf{T}_{\pi(\mathbf{e}_1+\mathbf{e}_2)} \right\rangle \simeq \left(\mathbf{D}_4 \ltimes (\mathbb{Z}/2N\mathbb{Z})^2\right)$ *if* $\theta_0 \in \frac{\pi}{2}\mathbb{Z}$.

2. $\Gamma = \left\langle \mathbf{R}^{\mathbf{p}_c}_{\phi_0}, \mathbf{T}_{\pi(\mathbf{e}_1+\mathbf{e}_2)} \right\rangle \simeq \left(\mathbf{C}_4 \ltimes (\mathbb{Z}/2N\mathbb{Z})^2\right)$ *otherwise.*

Finally, the subgroup of translation symmetries is the lattice:

$$\mathcal{L}\left[\pi\left(\mathbf{e}_1+\mathbf{e}_2\right), \pi\left(\mathbf{e}_1-\mathbf{e}_2\right)\right].$$

Proof. This is a direct consequences of the lemmas in the previous section. There is however a simplification in the square case, namely the translation $\mathbf{T}_{\pi(\mathbf{e}_1+\mathbf{e}_2)}$ is a symmetry. Indeed, using Lemma 3.1, it is straightforward to show that $\mathbf{J}_{LR}(\mathbf{T}_{\pi(\mathbf{e}_1+\mathbf{e}_2)}x, \mathbf{T}_{\pi(\mathbf{e}_1+\mathbf{e}_2)}y) = \mathbf{J}_{LR}(x,y)$. Note that the translation $\mathbf{T}_{\pi(\mathbf{e}_1+\mathbf{e}_2)}$ commutes with $\mathbf{T}_{2\pi\mathbf{e}_1}$ and $\mathbf{R}^{\mathbf{p}_c}_{\phi_0}$. Finally, let us show that $\mathbf{T}_{2\pi\mathbf{e}_1}$ is generated by the group elements listed in the lemma. Indeed, $\mathbf{T}_{\pi(\mathbf{e}_1-\mathbf{e}_2)} = (\mathbf{R}^{\mathbf{p}_c}_{\phi_0})^{-1}\mathbf{T}_{\pi(\mathbf{e}_1+\mathbf{e}_2)}$ and $\mathbf{T}_{2\pi\mathbf{e}_1} = \mathbf{T}_{\pi(\mathbf{e}_1-\mathbf{e}_2)} + \mathbf{T}_{\pi(\mathbf{e}_1+\mathbf{e}_2)}$.

To prove that the lattice of translations of the symmetry group is $\mathcal{L}\left[\frac{\pi}{2}(\mathbf{e}_1+\mathbf{e}_2), \frac{\pi}{2}(\mathbf{e}_1-\mathbf{e}_2)\right]$, we can look at (see lemma A.1) $\mathbf{R}^{\mathbf{b}}(\mathbf{R}^{\mathbf{a}})^{-1}\mathbf{x} = \mathbf{x} + (\mathbf{R}^{\mathbf{o}} - Id)(\mathbf{a}-\mathbf{b})$ which is a translation. Using the rotations with axis $\mathbf{a} = 0$ and $\mathbf{b} = \pi\mathbf{e}_1$ allows to conclude.

The previous result gives the generators of the group. These groups are very well known as crystallographic groups in the literature (see [Cox61, Mil72, Sch78] for an introduction). More precisely, we find that the symmetry group Γ of the equations, in the case $\chi, \epsilon_{LR} \neq 0$, is the crystallographic group P4M if $\theta_0 \in \frac{\pi}{2}\mathbb{Z}$ and P4 otherwise.

It is interesting to note that $\mathbf{D}_2$ is the point group associated to the PMM PO map whereas the point group of the network equations can be $\mathbf{D}_4$.

3.1.2 The hexagonal case

The main difference with the square case is that the clockwise rotation does not give a network symmetry because of the anisotropic function J_0 in (7) when $\chi > 0$. Hence, only half of the pinwheel are centers of rotation for the network equations (1), namely the counterclockwise pinwheels. A direct consequence of the lemmas in the previous section is:

Proposition 3.6 *For the (P3M1) PO map in Figure 2 b, the symmetry group* Γ *associated with the connectivity (7) in the case* $\chi > 0, \epsilon_{LR} \neq 0$ *is:*

1. $\Gamma = \left\langle \mathbf{K}, \mathbf{R}_{\phi_0}^{\mathbf{p}_{cc}}, \mathbf{T}^{-1}_{\frac{2\pi}{3}(e_1+e_2)} \mathbf{R}_{\phi_0}^{\mathbf{p}_c}, \mathbf{T}_{2\pi e_1} \right\rangle$ *if* $\theta_0 \in \frac{\pi}{2}\mathbb{Z}$
2. $\Gamma = \left\langle \mathbf{R}_{\phi_0}^{\mathbf{p}_{cc}}, \mathbf{T}^{-1}_{\frac{2\pi}{3}(e_1+e_2)} \mathbf{R}_{\phi_0}^{\mathbf{p}_c}, \mathbf{T}_{2\pi e_1} \right\rangle$ *otherwise.*

Finally, the subgroup of translation symmetries is the lattice: $\mathcal{L}[2\pi e_1, 2\pi e_2]$.

Proof. The only thing left to prove is about the lattice of translations. We can look at (see lemma A.1) $\mathbf{T}_{\mathbf{t}}^{-1}\mathbf{R}^{\mathbf{p}_c}(\mathbf{R}^{\mathbf{p}_{cc}})^{-1}\mathbf{x} = \mathbf{x} + (\mathbf{R}^{\mathbf{o}} - Id)(\mathbf{p}_{cc} - \mathbf{p}_c) - \mathbf{t}$ which is a translation where $\mathbf{t} \equiv \frac{2\pi}{3}(e_1 + e_2)$. When computed for $\mathbf{p}_{cc} - \mathbf{p}_c \in \{\frac{2\pi}{3}e_1, -\frac{2\pi}{3}e_2, -\frac{4\pi}{3}e_1, \frac{4\pi}{3}e_2\}$, we do not find a distinct sub-lattice of translations of $\mathcal{L}[2\pi e_1, 2\pi e_2]$.

As for the square lattice, we can identify the group in the hexagonal case. The symmetry group Γ of the equations, in the case $\chi, \epsilon_{LR} \neq 0$, is the crystallographic group P3M1 if $\theta_0 \in \frac{\pi}{2}\mathbb{Z}$ and P3 otherwise.

4 Forced symmetry-breaking of patterns

We now study the perturbation of the torus of translated states from V_0 when it is an attractor. It is well-known that in this case, a torus, flow-invariant manifold persists when the equations are perturbed, as long as the perturbations are small (and smooth) enough [CL00].

Our aim in this section is to determine how many steady-states do actually persist when the system is perturbed by turning on long-range connections $\epsilon_{LR} \neq 0$, and which phase portrait sets in on the perturbed torus.

Our method is as follows. We first analyze the remaining symmetries on the perturbed torus when $\epsilon_{LR} \neq 0$. This allows to assert the persistence of some steady-states (equilibria) which stand at points of maximal isotropy for the action of Γ on the perturbed torus. Moreover, when these isotropy subgroups contain the m-fold rotation group $\mathbf{C}_m$ with $m \geq 3$, these equilibria are foci (attractive or repulsive) or nodes (case when the Jacobian matrix has a double real eigenvalue). Now, the topology of the torus is an important constraint for the distribution of equilibria of saddle and other types. This follows from *Poincaré-Hopf theorem*, which can be found in an abundant literature and textbooks, and which can be stated as follows:

Theorem 4.1 *Let* $\mathcal{V}$ *be a compact orientable surface and suppose that all equilibria of a vector field defined on* $\mathcal{V}$ *are non-degenerate (i.e. hyperbolic: all eigenvalues of Jacobian matrices have non zero real part). Let* n *be the number of equilibria on* $\mathcal{V}$ *and* p *the number of those which are of* saddle *type (eigenvalues have opposite signs). Then* $n - 2p = \chi$*, the Euler characteristic of* $\mathcal{V}$.

In our case $\mathcal{V}$ is the torus, and hence $\chi = 0$. Therefore there are an equal number of equilibria of saddle type and of non saddle type. These two informations (symmetries and Poincaré-Hopf theorem) greatly help to classify the possible phase portraits on the torus. The idea of analyzing the dynamics on a group orbit of equilibria under symmetry-breaking perturbations

was introduced by [LR92]. It was applied in a theoretical setting to the case when the group orbit is a torus of square patterns [HG97] or hexagonal patterns [PGS06] with the aim of showing the existence of robust heteroclinic cycles under certain conditions. Our aim here is different and we only focus on the cases which correspond to our model.
We next consider the square case and the hexagonal case and we list the possible phase portraits of simplest type, that is with the minimal number of equilibria, assuming that these are the pictures which will naturally arise in our model, unless further degeneracies are assumed. Then numerical direct simulations of the dynamics on the perturbed torus allow us to fix the actual dynamics which is induced on the invariant tori when switching on the long-range connections.

4.1 On the perturbed torus

As the perturbed torus $\mathcal{T}_{\epsilon_{LR}}$ is diffeomorphic to the unperturbed torus $\mathcal{T}_0$, we can work in the coordinates of $\mathcal{T}_0$ for which the group action expression is known (see below). In the numerical experiments, the diffeomorphism is not known and thus, as we use $\mathcal{T}_0$ coordinates, the projection of the patterns on this coordinate system is only approximative (see Figure 3 for example).

To fix ideas, it is useful to be a bit more explicit. When $\epsilon_{LR} = 0$, we write the unperturbed torus as

$$\mathcal{T}_0 = \{V_0(\cdot - \mathbf{t}),\ \mathbf{t} \in \Omega\} \subset \mathrm{L}^2_{\mathrm{per}}(\Omega, \mathbb{R})$$

where V_0 is a stationary solution for $\epsilon_{LR} = 0$. We assume that the torus solution is invariant by rotation and reflection which is equivalent to assuming V_0 invariant by rotation and reflection. Under this assumption, the actions of rotations / reflections on the torus satisfy:

$$(\mathbf{R^o}, \mathbf{t}) \to \mathbf{R^o} \cdot \mathbf{t},\ (\mathbf{K}, \mathbf{t}) \to \mathbf{K} \cdot \mathbf{t} \tag{8}$$

This follows from $\mathbf{R^o T_t} \cdot V_0 = \mathbf{T}_{\mathbf{R^o t}} V_0$. It implies that the action of a rotation $\mathbf{R^a}$ of axis $\mathbf{a}$ is the given by:

$$(\mathbf{R^a}, \mathbf{t}) \to \mathbf{R^a} \cdot \mathbf{t}.$$

In our model, the lattice of translations symmetries of the torus matches the one of the PO map (see section 2). Hence, V_0 has the pinwheel periodicity:

$$V_0(\mathbf{x} + 2\pi k e_1 + 2\pi p e_2) = V_0(\mathbf{x}), \forall \mathbf{x} \in \Omega, \quad k, p \in \mathbb{Z}. \tag{9}$$

If we identify $V_0(\cdot - \mathbf{t})$ and $\mathbf{t}$, we can further simplify the study of the perturbed torus by decomposing $\mathbf{t}$ as follow:

$$\mathbf{t} = \phi_1 e_1 + \phi_2 e_2.$$

The assumption (9) implies that $\phi_i \in [0, 2\pi)$.

Remark 3 We cannot apply directly our method to the branch of stripes in Figure 1 neither to the branch of hexagonal patterns because the unperturbed torus generated by these patterns is not invariant by rotations.

4.2 Square case

Using the decomposition $\mathbf{t} = \phi_1 e_1 + \phi_2 e_2$, one finds:

$$\begin{cases} \mathbf{R^o} \cdot (\phi_1, \phi_2) & = (\ -\phi_2,\ \ \phi_1) \\ \mathbf{K} \cdot (\phi_1, \phi_2) & = (\ \ \phi_1,\ -\phi_2) \end{cases} \tag{10}$$

We collect the main results concerning the dynamics on the square in the following proposition. It is the backbone for determining the possible phase portraits on the perturbed torus.

Proposition 4.2 *Let us assume that there is a finite number of equilibria on the perturbed torus which are all non-degenerate when $\epsilon_{LR} \neq 0, \chi \geq 0$. For the lattice PMM, there are at least 8 equilibria on the perturbed torus $\mathcal{T}_{\epsilon_{LR}}$, 4 of which are saddle and the other 4 are nodes / foci, they are given by:*

$$Fix(\langle(\mathbf{R^o})^2\rangle) \quad = \quad \{(0,0),\ (0,\pi),\ (\pi,0),\ (\pi,\pi)\} \tag{11}$$

which are centers of rotation,

Proof. It is easy to prove (11). Fixed point subspaces are flow invariant, this implies that $Fix(\langle\mathbf{R}_s^2\rangle)$ is composed of stationary solutions. We also note that:

$$Fix(\langle\mathbf{R^o}\rangle) = \{(0,0),\ (\pi,\pi)\}\,.$$

We write $\frac{d}{dt}\phi = F(\phi)$ the dynamics on the torus. The equivariance implies that $dF(\gamma\cdot\phi)\gamma = \gamma\cdot dF(\phi)$. As $\phi \in Fix(\langle\mathbf{R^o}\rangle)$ is Γ-invariant, it implies that $dF(\phi)$ commutes with the rotation (10). Simple linear algebra shows that $dF(\phi)$ must be a rotation matrix, *i.e.* that $Fix(\langle\mathbf{R^o}\rangle)$ is composed of nodes/foci. It remains to show that this is also true for $(0,\pi)$ and $(\pi,0)$. This follows from Lemma 3.4 and

$$\mathbf{T}^{-1}_{\pi(e_1+e_2)}\mathbf{R^o}\cdot(0,\pi) = (0,\pi).$$

As $\mathbf{R^o}$ and $\mathbf{T}_{\pi(e_1+e_2)}$ commute, $\mathbf{T}^{-1}_{\pi(e_1+e_2)}\mathbf{R^o}$ is of order 4, hence it is the rotation of center $(0,\pi)$. Now, we can see the action of $\mathbf{T}^{-1}_{\pi(e_1+e_2)}\mathbf{R^o}$ on the manifold $\mathcal{T}_0$ is affine. Writing $\gamma \equiv \mathbf{T}^{-1}_{\pi(e_1+e_2)}\mathbf{R^o}$, the equivariance gives

$$d\gamma(F(0,\pi))dF(0,\pi) = dF(\gamma(0,\pi))d\gamma(0,\pi).$$

From γ being affine and $(0,\pi) \in Fix\gamma$, we find that $dF(0,\pi)$ commute with $d\gamma = d\mathbf{R}^o$ seen as a map on the torus. This allows to conclude that $(0,\pi)$ is a node/focus, and also $(\pi,0)$. Being fixed points of rotations, the 4 nodes/foci are center of rotation symmetry.

Assume now that there are a finite number of zeros $(\phi_i)_{i=1\cdots n}$ on $\mathcal{T}_{\epsilon_{LR}}$ which are all non-degenerate. Thanks to theorem 4.1

$$\sum_{i=1}^{n} sign\det dF(\phi_i) = 0$$

This gives

$$-4 = \sum_{\phi_i\notin Fix(\mathbf{R}_s^2)} sign\det dF(\phi_i)$$

which implies the existence of at least 4 saddles.

A convenient way to find the foci is to look at the fundamental domain in Figure 2 a. These foci corresponds to the pinwheels in the fundamental domain.

We have seen that the minimal configuration, under the hypothesis that all equilibria on the perturbed torus are hyperbolic, is that of eight equilibrium points with four foci and four saddles. How does the associated phase portrait look like on the torus? The answer crucially depends upon the presence of reflection symmetry (case when $\theta_0 = 0$). In this case the axes of reflection symmetry pass by the equilibria. Therefore the foci are necessarily of node type: the eigenvalues of the Jacobian are double and real. The axes of reflection symmetry are invariant by the flow, which constrains the phase portrait to the scheme shown in Fig. 3. On the other hand when there is no reflection symmmetry the foci are typically "true" foci: the eigenvalues of

the Jacobian are complex conjugate. This allows for the possibility of periodic orbits centered at such foci, as shown in Fig. 4. These two typical situations are observed numerically, as shown on the right pictures in Fig. 3 and 4.

In order to observe limit cycles numerically, we had to change the connectivity. Indeed, if we use the prefactor $G_{\sigma_\theta} = \cos$ in (7), the imaginary part of the eigenvalues of the equilibria coming from the breaking of the reflection symmetry by choosing $\theta_0 \notin \frac{\pi}{2}\mathbb{Z}$ are tiny: at least 3 orders of magnitude smaller than the real part. In effect, even if we beak the reflection symmetry, we observe a dynamics similar to the one in Fig. 3. To have larger imaginary part, we connect neurons with opposite preferred orientation by choosing the prefactor $G_{\sigma_\theta} = \sin$ in (7). We further choose the connectivity with largest imaginary part among connectivities in B. Note that despite varying almost all parameters, we only observed the two situations as in Fig. 3 and 4 (up to a time reversal of the absence of limit cycles), as if naturally, the network equations (1) produce the simplest possibilities for all parameters that we investigated.

Remark 4 We would like to mention that great care was taken to code the equivariance and that numerically, the error of symmetries was around $1e-16$ *for the 2-norm of an arbitrary vector of 2-norm around* 37*. This allows to check the predicted values of the stationary points with great accuracy using Newton algorithm. In particular, we find numerically in Fig. 3 that the points* $(\mathbf{R}^{\mathbf{o}})^k \cdot \left(\frac{\pi}{2}, 0\right), k = 0, \cdots, 3$ *are indeed saddle points.*

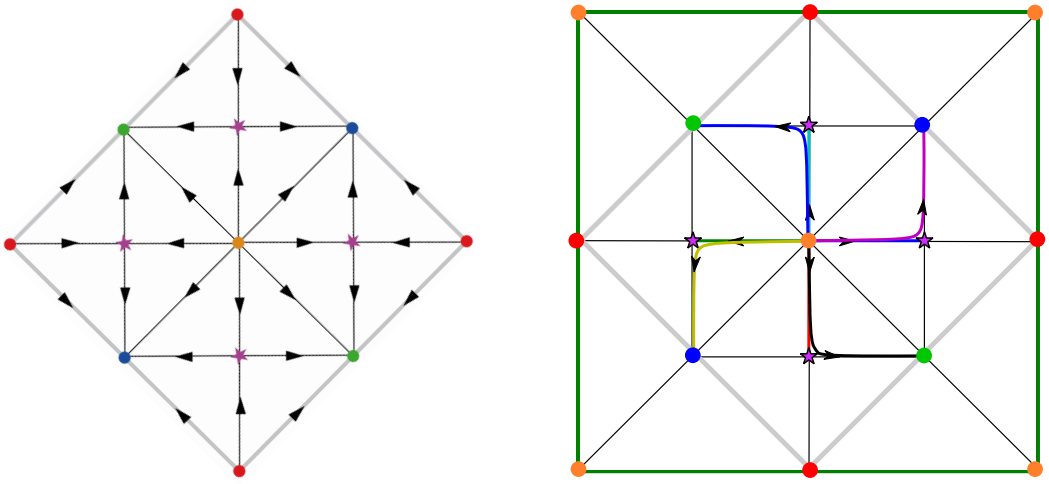

Figure 3: Example of dynamics for the PO map in Figure 2 a in the case where $\Gamma = \langle \mathbf{R}_s, \mathbf{T}_{0,2\pi} \rangle$ and $\theta_0 = 0$. Left: sketch of the phase portrait in the fundamental domain. Right: eight numerical trajectories of (1) projected on the unperturbed torus $\mathcal{T}_0$. The fundamental domain is superimposed to compare with prediction. Parameters are as follow: connectivity $J^{p,r}_{LR}(\mathbf{x}, \mathbf{y})$ (see appendix B), $\epsilon_{LR} = 0.001, \chi = 0.9$ and $\sigma = 1.06264$. The size of the cortex is $4 \times 2\pi$. The number of unknowns is 1024^2.

4.3 Hexagonal case

We now consider the hexagonal lattice. This case is different from the square lattice because it seems from Proposition 3.6 that only counterclockwise pinwheels are center of rotations. However,

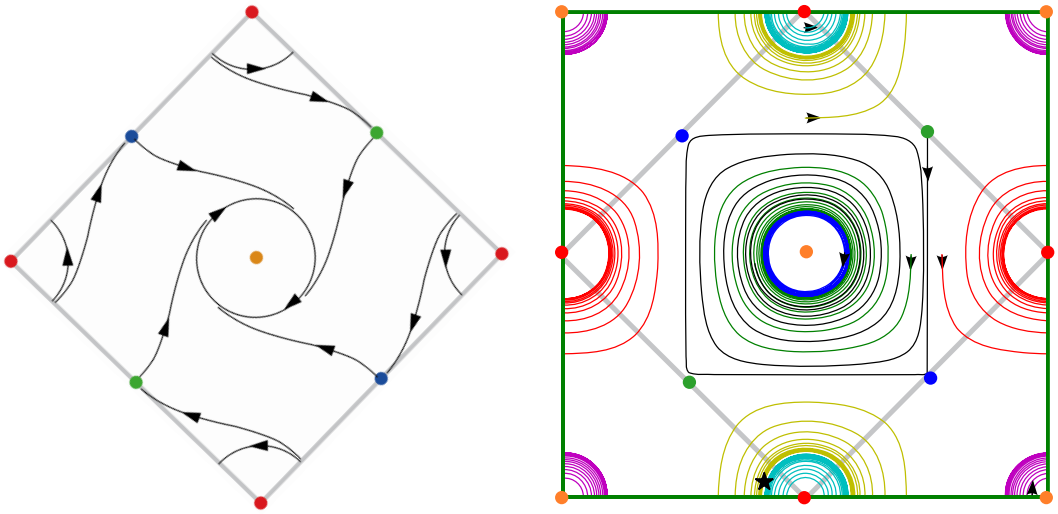

Figure 4: Example of dynamics for the PO map in Figure 2 a in the case where $\Gamma = \langle \mathbf{R}_s, \mathbf{T}_{0,2\pi} \rangle$ and $\theta_0 \notin \frac{\pi}{2}\mathbb{Z}$. Left: simplest dynamics found in this case shown in the fundamental domain. Right: Numerical solution of (1) projected on the unperturbed torus $\mathcal{T}_0$. The fundamental domain is superimposed to compare with prediction. Parameters are as follow: connectivity $J_{LR}^{b,a}(\mathbf{x},\mathbf{y})$ (see appendix B), $\epsilon_{LR} = 0.001, \chi = 0.9$ and $\sigma = 1.06264$. The size of the cortex is $4 \times 2\pi$. The number of unknowns is 1024^2.

it turns out that γ as in Lemma 3.4 is a rotation on the torus, hence yielding the other pinwheels as center of rotations.

We shall use a different way of proving the current proposition rather than the method adopted for proposition 4.2. Using a decomposition $\mathbf{t} = \phi_1 e_1 + \phi_2 e_2$, one finds

$$\mathbf{R}^{\mathbf{p}} \cdot \mathbf{t} = \begin{bmatrix} 2p_1 + p_2 - \phi_1 - \phi_2 \\ \phi_1 - p_1 + p_2 \end{bmatrix}, \mathbf{p} = p_1 e_1 + p_2 e_2.$$

Proposition 4.3 *Let us assume that there is a finite number of equilibria on the perturbed torus which are all non-degenerate when $\epsilon_{LR} \neq 0, \chi \geq 0$. For the lattice P3M1, there are at least 18 equilibria on the perturbed torus $\mathcal{T}_{\epsilon_{LR}}$, 9 of which are saddle and the other 9 are nodes/foci, given by the lattice $\mathcal{L}\left[\frac{2\pi}{3}e_1, \frac{2\pi}{3}e_2\right]$ which are centers of rotation. The subgroup of translation symmetries is the lattice $\mathcal{L}\left[\frac{2\pi}{3}(\mathbf{e}_1 + \mathbf{e}_2), \frac{2\pi}{3}(-\mathbf{e}_1 + 2\mathbf{e}_2)\right]$*

Proof. In the fundamental domain, only counterclockwise pinwheels lead to a rotational symmetry. The centre of rotation is then a node/focus point. In particular, we find the following node/foci points (see section 3.1.2 for a definition)

$$(\phi_1, \phi_2) \in \left\{ \left(\frac{4\pi}{3}, 0\right), \left(\frac{2\pi}{3}, \frac{4\pi}{3}\right), \left(0, \frac{2\pi}{3}\right) \right\}.$$

We now have a look at the symmetry $\gamma \equiv \mathbf{T}^{-1}_{\frac{2\pi}{3}(e_1+e_2)} \mathbf{R}^{\mathbf{p}_c}$ defined in Proposition 3.6 where the axis of rotation is $\mathbf{p}_c = \frac{2\pi}{3}(2e_1 + e_2)$. On the hexagonal torus, we find that $\gamma = \mathbf{R}^{\mathbf{o}}$ which can be seen by writing the equations in the basis e_1, e_2. It yields $Fix(\gamma) = \left(\frac{\pi}{3}, \frac{\pi}{3}\right)\mathbb{Z}$. Hence, these points are equilibria of node/foci type. It gives 3 additional nodes/foci.

Now, we can use these centers of rotation to rotate each node/foci to find other equilibria. Using Lemma A.2, we have $\gamma = \mathbf{R}^{\mathbf{v}} \cdot \mathbf{R}^{\mathbf{o}} = (\mathbf{R}^{\mathbf{u}})^{-1}$ where $\mathbf{v} = \frac{2\pi}{3}(e_1 + 2e_2)$ and $\mathbf{u} = \frac{4\pi}{3}e_2$. This leads the additional centers of rotations (hence node/foci):

$$(\phi_1, \phi_2) \in \left\{ \left(\frac{2\pi}{3}, 0\right), \left(0, \frac{4\pi}{3}\right), \left(\frac{4\pi}{3}, \frac{2\pi}{3}\right) \right\}.$$

It follows that there are (at least) 9 foci. Assuming now that there are a finite number of zeros on $\mathcal{T}_{\epsilon_{LR}}$ which are all non-degenerate, theorem 4.1 implies that there are as many saddles as foci.

We have shown that $\mathcal{L}\left[\frac{2\pi}{3}e_1, \frac{2\pi}{3}e_2\right]$ is composed of centers of rotation. Using again Lemma A.1 with $\mathbf{a} - \mathbf{b} \in \mathcal{L}\left[\frac{2\pi}{3}e_1, \frac{2\pi}{3}e_2\right]$, we find that the subgroup of translation symmetries is given by $\mathcal{L}\left[\frac{2\pi}{3}(\mathbf{e}_1 + \mathbf{e}_2), \frac{2\pi}{3}(-\mathbf{e}_1 + 2\mathbf{e}_2)\right]$.

We take the opportunity to show how the different nodes/foci found in proposition 3.6 can be interpreted in cortical coordinates, as shown in Figure 5. Briefly, we superimpose by transparency the cortical activity over the PO map θ (transparent mean that the cortical activity is high). We then plot little edges or patches depending on whether a subset of the hypercolumn is activated or not.

As in the square case, we can deduce from these results the phase portrait when assuming that the equilibria on the perturbed torus are all hyperbolic and that there are exactly 18 of them, nine foci and nine saddles. The situation is slightly more complicated than in the square case, however it is not difficult to show that a typical phase portrait looks like one of the diagrams shown in Fig. 6. It is numerically checked that this "minimal" situation is indeed occurring. There a periodic orbit was assumed to exist around the focus in the center of the domain, but this is unnecessary.

As in the square case, we had to use $G_{\sigma_\theta} = \sin$ in order to see foci with non vanishing rotation number. Compared to the square case, we had great trouble ensuring the different symmetries numerically. The error of equivariance is a least 3 orders of magnitude bigger than for the square lattice and given that we need to numerically solve (1) for very long time, the error of symmetries seem to build up. Nevertheless, we can still produce simulations which satisfies the hypothesis of our model as the one in Fig.6. Except for the points $\left(\frac{2\pi}{3}, \frac{2\pi}{3}\right)\mathbb{Z}$, we find the stationary points predicted by prop. 3.6 using Newton algorithm. Around the points $\left(\frac{2\pi}{3}, \frac{2\pi}{3}\right)\mathbb{Z}$, the Newton algorithm did not converge and it seems to be caused by the presence of the saddle points (also predicted in prop. 3.6). Indeed, this can be hinted by the kinks on the trajectories around orange points.

In the numerical simulation displayed in Fig.7, no periodic orbit is found. On the other hand, we observe the remarkable fact that the simulations also lead to simplest possible scenarios with smallest number of stationary points and periodic solution.

5 Discussion

In this work, we have extended the seminal and very influential work [BCG+01] on cortical hallucinations after the original work of Ermentrout and Cowan [EC79]. Our idea is to assume a discrete lattice of pinwheels (as opposed to a continuous one) and to describe the cortical activity in the laminar zone which is located in between pinwheels. This is important for example if we want to confront our predictions to optical imaging experiments. This approach has led us to shed some new light onto two outstanding questions; what are the possible lattices of pinwheels? they turn out to be closely related to the wallpaper groups; what is the simplest spontaneous dynamics generated by these networks? they turn out to be determined by the perturbation of invariant tori.

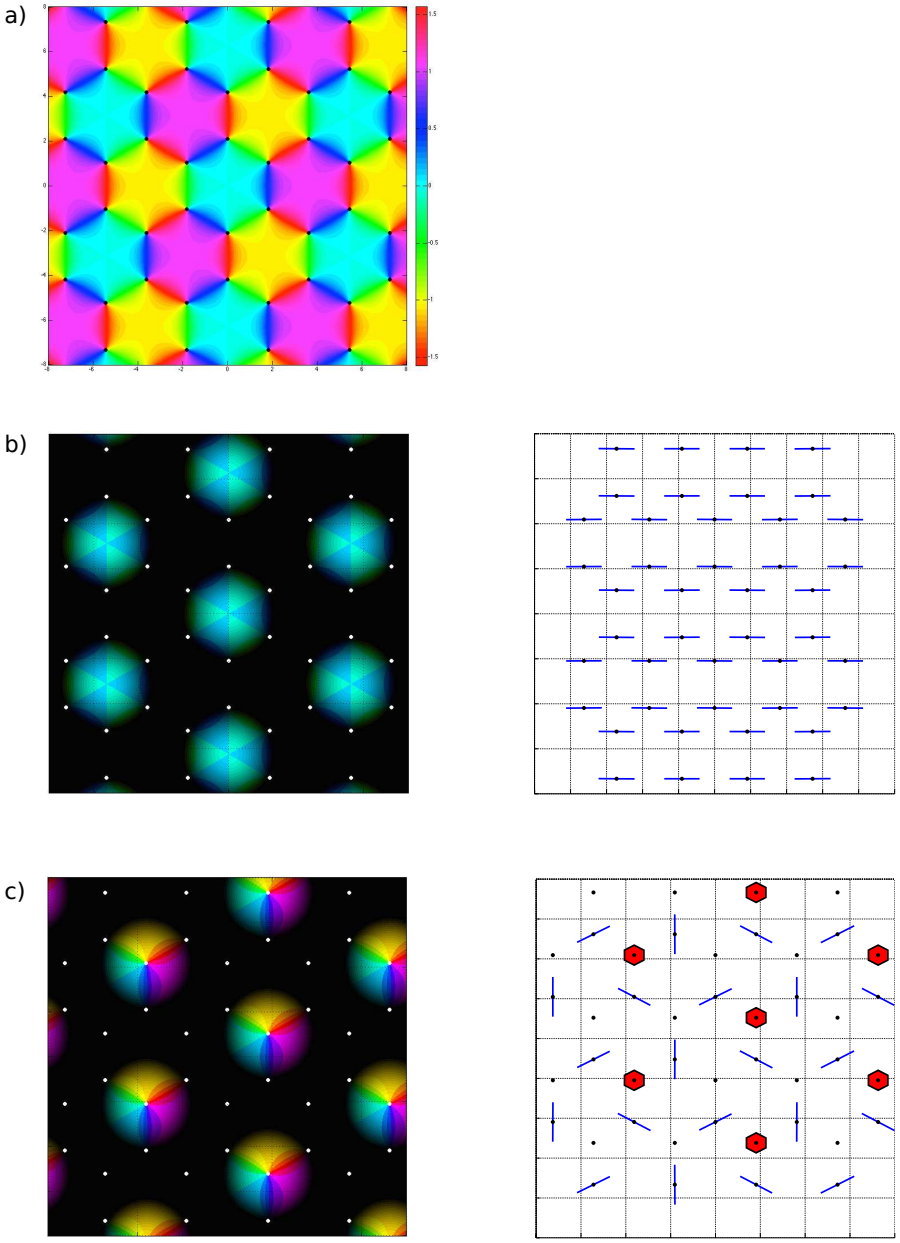

Figure 5: Left: example of cortical activation shown in transparent, over an hexagonal P3M1 PO map. We show two particular activations as predicted by prop. 3.6. The pinwheels are shown in white. Right: interpretation of such activation in cortical coordinates made by pooling the different activated orientations around each pinwheel.

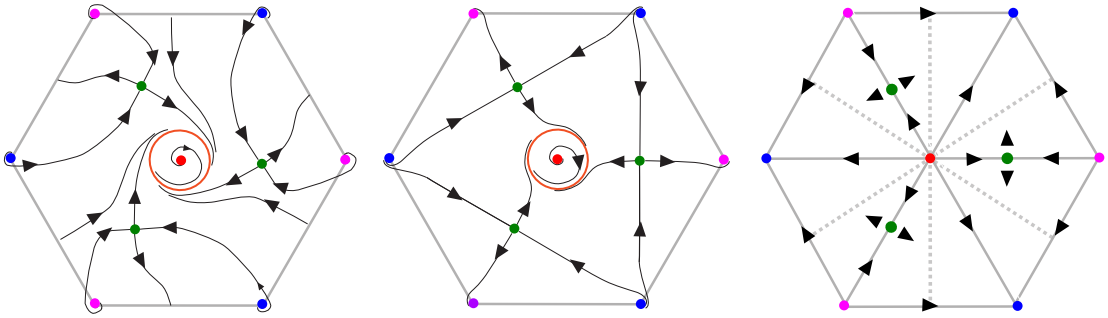

Figure 6: Sketch of the phase portrait on the perturbed torus. Two cases (left) are shown, assuming that a periodic orbit surrounds the focus at the center. Another case (right) is shown in the case of reflexion symmetry. The presence or absence of periodic orbits is essentially related to the sign of the real part of the eigenvalues of the Jacobian at the central focus.

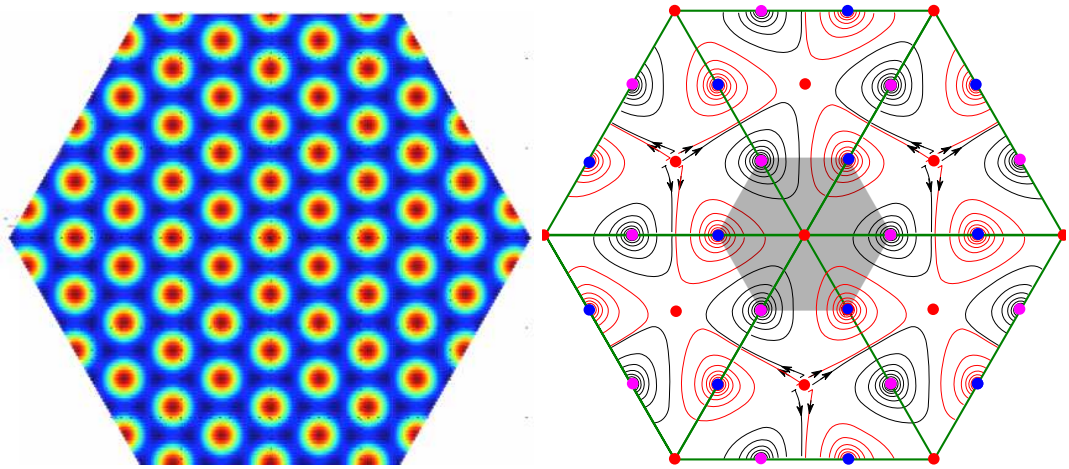

Figure 7: Left: example of solution on the unperturbed torus $\mathcal{T}_0$ obtained with Newton algorithm. Right: Numerical solution of (1) projected on the unperturbed torus $\mathcal{T}_0$. The gray hexagon is the fundamental domain from Prop. 4.3. The bottom right parallelogram is the result of 6 simulations, the hexagon was built by tiling this parallelogram. Parameters are as follow: connectivity $J^{p,a}_{LR}(\mathbf{x},\mathbf{y})$ (see appendix B), $\epsilon_{LR} = 0.5, \chi = 0.2$ and $\sigma = 1.11264$. The size of the cortex is $8 \times 2\pi$. The number of unknowns is $3 \cdot 1024^2$.

The first question is natural but, to the best of our knowledge, has never been addressed theoretically despite the fact that it allows to apply the equivariant theory of dynamical systems in a very similar way to [BCG$^+$01] albeit in a more biologically plausible setting. In [WG98] the authors describe a mechanism that allows them to describe the probability of observing a network of pinwheels with a given density but because their equations are driven by white noise they lose all symmetries.

The second question is more subtle and in effect stems from numerical work where we found very difficult to implement the ideas of [BCG$^+$01, Bre03], at least for a square cortex. The computation of the bifurcation diagram in Figure 1 led us to study the perturbation of solutions that were not close to bifurcation points (see the brown lines in Figure 1), indeed this accounts for the most probable dynamics. As such, the bifurcation diagram Figure 1 is an indication of the difficulty to apply the theory developed in [BCG$^+$01] of cortical hallucinations where it was assumed, that such stereotyped cortical patterns could be explained by adjusting the network parameters close to bifurcation points. Indeed, in such a setting, the validity of the theory shrinks rapidly with the size of the cortex and, as far as we know, for all practical purpose it is difficult to use it to account for observations. The problem is the same with [Bre03] in which the authors study the perturbation of a system close to a bifurcation with spatial forcing close to resonance. Secondary bifurcations might seriously restrict the validity of the approach.

Let us examine the impact of our investigations onto our current understanding of the functioning of V1. The first consequence can be drawn from Figure 1, the hexagonal case is the 'only' robust one from a modeling point of view. Indeed, even with the square lattice, the branches which are stable over an extended parameter set, have a near hexagonal symmetry. Hence, there is a mismatch between the solution approximate symmetry and the network symmetry that is only resolved in the case of the hexagonal pinwheel lattice. The second consequence is that, within the class of pinwheel lattices that we consider, those displaying the reflection symmetry are non-generic (see section 3). This has the consequence of producing foci and (possibly) limit cycles as described in propositions 4.2 and 4.3. This is different from [BCG$^+$01] where all bifurcated patterns are stationary. Note that [GST03] reports time-periodic states in model similar to [BCG$^+$01] but with additional symmetry. The last consequence of our work is that it allows a generalization of both theories [EC79, BCG$^+$01]. Indeed, the first theory allows the description of non-contoured cortical spontaneous activations like in Figure 8 a-b. The second theory generalizes the first one by allowing the prediction of contoured patterns such as in in Figure 8 c as well as the non-contoured ones. Our theory describes contoured and non-contoured patterns as well as a mixture of such activation patterns as depicted in Figure 5 c.

Our work can be extended in several ways. First, there is a need for a bifurcation study of the dynamics on the torus w.r.t. the parameters ϵ_{LR}, χ, etc... Indeed, we have not been very quantitative concerning the role of these parameters in shaping the dynamics. There are also lattices that have not been investigated (CMM, P4M and P6M in Figure 2) and it would be interesting to study the kind of planforms they can produce. We have not looked at the case where the stripes are stable in the $\mathbf{D}_4$-pitchfork. That would be a minor modification of the present work but it would show another type of planforms. More generally, we have not discussed the cases where the unperturbed solution is a circle rather than a torus. Hence, it is desirable to classify the different planforms that can be produced from the unperturbed invariant manifolds for the different lattices. Another extension concerns the study of cases where the lattice of symmetry of the unperturbed torus $\mathcal{T}_0$ and the pinwheel lattice differ. The perturbation from the long-range connections would act as a periodic forcing on the unperturbed torus. Some models are available [Bre03, BC09] but we believe that they lack an important component which is synaptic plasticity. A relatively simple extension would be to consider the effect of synaptic/propagation delays [HBW03, Vel13]. Synaptic delays [RBH05] will not affect the unperturbed torus but

are likely to increase the imaginary part of the eigenvalues which we found otherwise nonzero albeit small when the reflection symmetry is broken. Other very exciting extensions concern the modeling of the spatial frequency tuning and the ocular dominance domains. It would be very interesting to re-visit some recent work on binocular rivalry [WBL01, KLK+10] in the light of the conclusions presented in this paper.

6 Acknowledgments

We would like to thank Paul Bressloff for useful comments and discussions. We also would like to warmly thank Dr. Huiyuan Li for providing their library of Fast Fourier Transform on hexagonal lattice as described in [LS05].
This work was partially supported by the European Union Seventh Framework Programme (FP7/2007-2013) under grant agreement no. 269921 (BrainScaleS), no. 318723 (Mathemacs), and by the ERC advanced grant NerVi no. 227747.

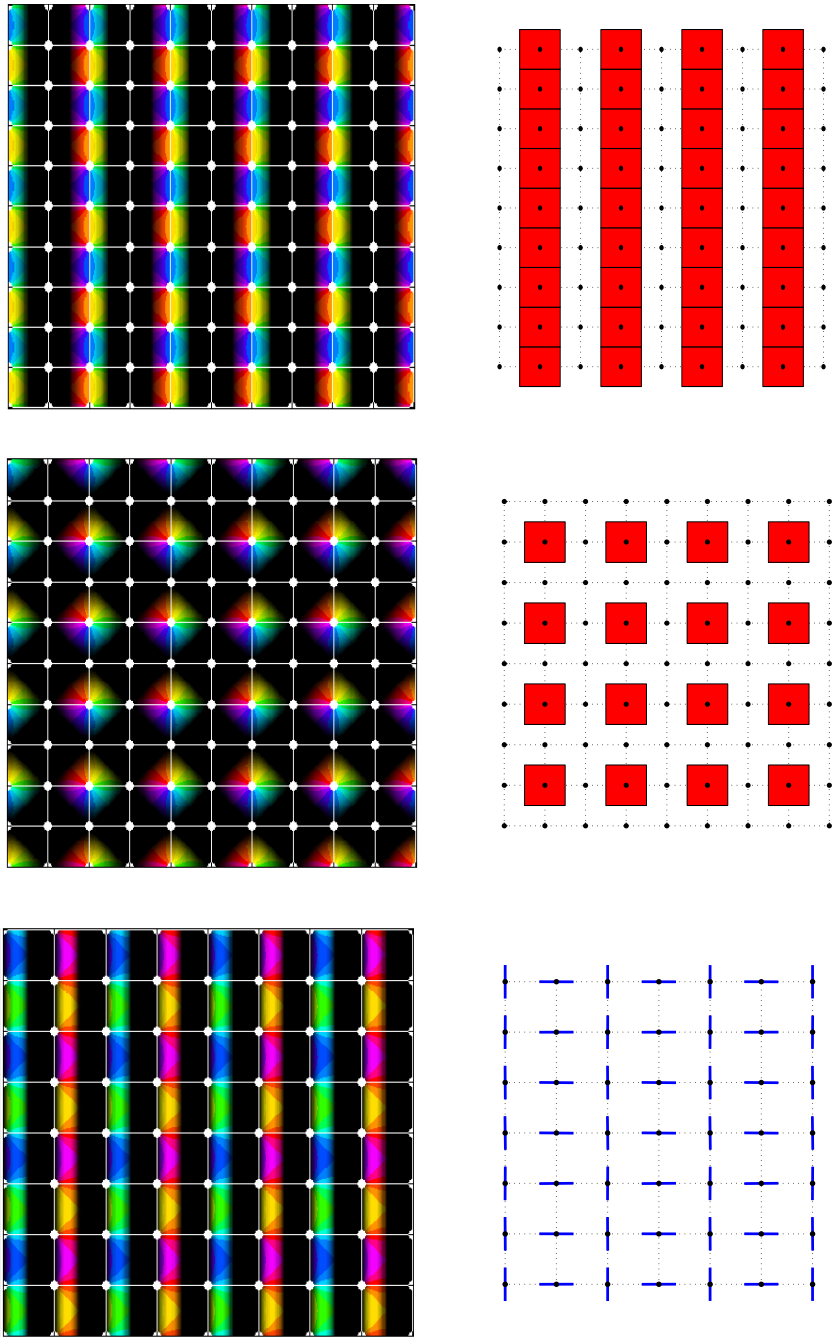

Figure 8: Left: example of cortical activation shown in transparent, over a PMM PO map. The pinwheels are shown in white. Right: interpretation of such activation in cortical coordinates made by pooling the different activated orientations around each pinwheel.

A Useful results

Lemma A.1 (Composition of rotations) *Let* $\mathbf{R^a}$ *(respectively* $\mathbf{R^b}$*) be the rotation of axis* $\mathbf{a}$ *(respectively* $\mathbf{b}$*). Let* $\mathbf{R^o}$ *be the rotation by the same angle through the origin. Then*

$$\mathbf{R^b}(\mathbf{R^a})^{-1}\mathbf{x} = \mathbf{x} + (\mathbf{R^o} - Id)(\mathbf{a} - \mathbf{b}).$$

Proof. Straightforward using $\mathbf{R^a}(\mathbf{x}) = \mathbf{R^o}(\mathbf{x} - \mathbf{a}) + \mathbf{a}$ and $(\mathbf{R^a})^{-1}(\mathbf{x}) = (\mathbf{R^o})^{-1}(\mathbf{x} - \mathbf{a}) + \mathbf{a}$.

Lemma A.2 *Let* $\mathbf{R}_h^{\mathbf{v}}$ *the hexagonal rotation of angle* $\frac{2\pi}{3}$ *and axis* $\mathbf{v}$ *acting on the hexagonal torus. Then, we have:*

$$\mathbf{R}_h^{\mathbf{v}} \cdot \mathbf{R}_h^{\mathbf{o}} = (\mathbf{R}_h^{\mathbf{u}})^{-1}, \quad \mathbf{u} = (v_1 + v_2, -v_1).$$

Proof. This is elementary algebra when writing the expression of the rotation in the basis $(\mathbf{e}_1, \mathbf{e}_2)$.

B Numerical experiments

The bifurcation diagram in Figure 1 was computed with the library Trilinos [HBH+03] using the FFTw library to compute the FFT on the square lattice. The method implements a Newton-Krylov solver with GMRES linear solver, the eigensolver is based on the Arnoldi algorithm. For the simulation of the full network, we follow [Bre03] to make the connectivity amenable to fast computations, *e.g.* using FFTs. Indeed, neglecting G_{σ_θ} in (7), we find

$$J_{LR}(\mathbf{x}, \mathbf{y}) = \sum_{k=1}^{3} D_k(\mathbf{x}) J_k(\mathbf{x} - \mathbf{y}) J(\mathbf{x} - \mathbf{y}) \tag{12}$$

where the mask $J(\mathbf{x}) = \mathbf{1}(\|\mathbf{x}\| < 3 \cdot 2\pi) - \mathbf{1}(\|\mathbf{x}\| > 1 \cdot 2\pi)$ allows to select long-range connections but no local connections. We use two different schemes, the one from [Bre03] (modified by multiplying the PO map θ by -1 to induce co-circular preferred connections) and another one found by Taylor expanding J_0 in (7):

$$D_1^{(b)}(\mathbf{x}) = \chi \cos^2\theta(\mathbf{x}),\ D_2^{(b)}(\mathbf{x}) = 2\chi \cos\theta(\mathbf{x}) \sin\theta(\mathbf{x}),\ D_3^{(b)}(\mathbf{x}) = \chi \sin^2\theta(\mathbf{x})$$
$$J_1^{(b)}(\mathbf{x}) = x_1^2 J(\mathbf{x}),\ J_2^{(b)}(\mathbf{x}) = x_1 x_2 J(\mathbf{x}),\ J_3^{(b)}(\mathbf{x}) = x_2^2 J(\mathbf{x}) \tag{13}$$

and

$$D_1^{(p)}(\mathbf{x}) = \cos^2\theta(\mathbf{x}),\ D_2^{(p)}(\mathbf{x}) = -2\cos\theta(\mathbf{x}) \sin\theta(\mathbf{x}),\ D_3^{(p)}(\mathbf{x}) = \sin^2\theta(\mathbf{x})$$
$$J_1^{(p)}(\mathbf{x}) = (1-\chi)x_1^2 + x_2^2,\ J_2^{(p)}(\mathbf{x}) = x_1 x_2,\ J_3^{(p)}(\mathbf{x}) = x_1^2 + (1-\chi)x_2^2. \tag{14}$$

In order to take into account the angular selection in $G_{\sigma_\theta}(\theta(\mathbf{x}) - \theta(\mathbf{y}))$ which is costly to compute, we introduce the following approximation

$$J_{\sigma_\theta}^{(regular)}(\mathbf{x}, \mathbf{y}) \equiv \cos(\theta(\mathbf{x}) - \theta(\mathbf{y})) = \cos(\theta(\mathbf{x}))\cos(\theta(\mathbf{y})) + \sin(\theta(\mathbf{x}))\sin(\theta(\mathbf{y}))$$

or

$$J_{\sigma_\theta}^{(anti)}(\mathbf{x}, \mathbf{y}) \equiv \sin(\theta(\mathbf{x}) - \theta(\mathbf{y})) = \sin(\theta(\mathbf{x}))\cos(\theta(\mathbf{y})) - \cos(\theta(\mathbf{x}))\sin(\theta(\mathbf{y})).$$

We note that $J_{\sigma_\theta}^{(regular)}$ connects neurons with similar preferred orientation whereas $J_{\sigma_\theta}^{(anti)}$ connects neurons whose preferred orientation differ by $\pm\pi$. The reason why we introduce this last

connectivity scheme is because it allows to have relatively large complex components in the eigenvalues of the jacobian at fixed points, which speeds up the dynamics on the invariant torus. To sum up, we use the connectivity function

$$J_{LR}^{num}(\mathbf{x},\mathbf{y}) = J_{\sigma_\theta}(\mathbf{x},\mathbf{y}) J_{LR}(\mathbf{x},\mathbf{y})$$

where J_{LR} is given by (12). It is found that this function satisfies

$$J_{LR}^{num}(\mathbf{x},\mathbf{y}) = \sum_{k=1}^{6} D_k^{'}(\mathbf{x}) J_k^{'}(\mathbf{x}-\mathbf{y}) C_k(\mathbf{y})$$

which is computationally very efficient. In the simulations, we use the following connectivities:

$$\begin{aligned} J_{LR}^{b,r}(\mathbf{x},\mathbf{y}) &\equiv J_{\sigma_\theta}^{(regular)}(\mathbf{x},\mathbf{y}) \sum_{k=1}^{3} D_k(\mathbf{x})^{(b)} J_k^{(b)}(\mathbf{x}-\mathbf{y}) J^{(b)}(\mathbf{x}-\mathbf{y}) \\ J_{LR}^{b,a}(\mathbf{x},\mathbf{y}) &\equiv J_{\sigma_\theta}^{(anti)}(\mathbf{x},\mathbf{y}) \sum_{k=1}^{3} D_k(\mathbf{x})^{(b)} J_k^{(b)}(\mathbf{x}-\mathbf{y}) J^{(b)}(\mathbf{x}-\mathbf{y}) \\ J_{LR}^{p,a}(\mathbf{x},\mathbf{y}) &\equiv J_{\sigma_\theta}^{(anti)}(\mathbf{x},\mathbf{y}) \sum_{k=1}^{3} D_k(\mathbf{x})^{(p)} J_k^{(p)}(\mathbf{x}-\mathbf{y}) J^{(p)}(\mathbf{x}-\mathbf{y}). \end{aligned} \tag{15}$$

In order to solve the differential equations (1) with a large number of unknowns, we use PETSc [BAA+14] and its Python extension PETSc4py [DPKC11]. The linear solver in this case is a deflated-GMRES combined with the BDF (backward differentiation formulas) method suitable for stiff systems. The simulations for the square lattice have 1024^2 unknowns, those for the hexagonal lattice have $3 \cdot 1024^2$.

References

[ALW+02] A. Angelucci, J.B. Levitt, E.J. Walton, J.M. Hupe, J. Bullier, and J.S. Lund. Circuits for local and global signal integration in primary visual cortex. *The Journal of Neuroscience*, 22(19):8633–8646, October 2002.

[BAA+14] Satish Balay, Shrirang Abhyankar, Mark F. Adams, Jed Brown, Peter Brune, Kris Buschelman, Victor Eijkhout, William D. Gropp, Dinesh Kaushik, Matthew G. Knepley, Lois Curfman McInnes, Karl Rupp, Barry F. Smith, and Hong Zhang. PETSc Web page. http://www.mcs.anl.gov/petsc, 2014.

[BC02] P.C. Bressloff and J.D. Cowan. The visual cortex as a crystal. *Physica D: Nonlinear Phenomena*, 173(3–4):226–258, December 2002.

[BC09] Tanya I Baker and Jack D Cowan. Spontaneous pattern formation and pinning in the primary visual cortex. *Journal of Physiology-Paris*, 103(1):52–68, 2009.

[BCG+01] P.C. Bressloff, J.D. Cowan, M. Golubitsky, P.J. Thomas, and M.C. Wiener. Geometric visual hallucinations, euclidean symmetry and the functional architecture of striate cortex. *Phil. Trans. R. Soc. Lond. B*, 306(1407):299–330, March 2001.

[Bre03] P.C. Bressloff. Spatially periodic modulation of cortical patterns by long-range horizontal connections. *Physica D: Nonlinear Phenomena*, 185(3-4):131–157, 2003.

[BS86] G.G. Blasdel and G. Salama. Voltage-sensitive dyes reveal a modular organization in monkey striate cortex. *Nature*, 321:579—585, 1986.

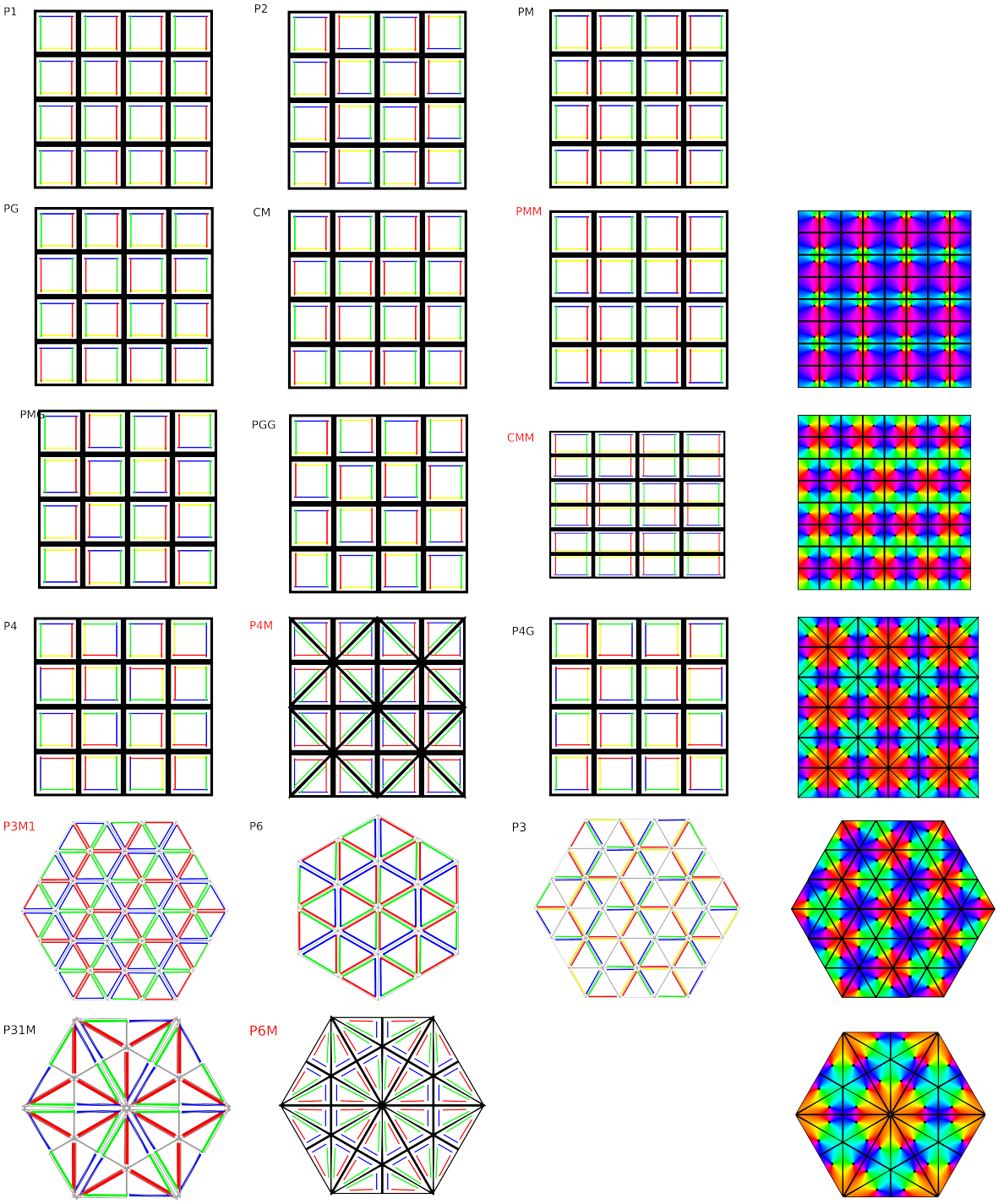

Figure 9: 17 possible tilings. Each element (square, triangle) represents an hypercolumn with a pinwheel at its center. The colored edges represent a coarse preferred orientation domain. Biologically plausible tilings are highlighted in red and a better representation is then produced on the same line.

[CL00] P. Chossat and R. Lauterbach. *Methods in Equivariant Bifurcations and Dynamical Systems*. World Scientific Publishing Company, 2000.

[Cox61] Harold Scott Macdonald Coxeter. *Introduction to geometry*. New York, London, 1961.

[DKM+95] R.J. Douglas, C. Koch, M. Mahowald, KA Martin, and H.H. Suarez. Recurrent excitation in neocortical circuits. *Science*, 269(5226):981, 1995.

[DPKC11] Lisandro D Dalcin, Rodrigo R Paz, Pablo A Kler, and Alejandro Cosimo. Parallel distributed computing using python. *Advances in Water Resources*, 34(9):1124–1139, 2011.

[EC79] GB Ermentrout and JD Cowan. A mathematical theory of visual hallucination patterns. *Biological Cybernetics*, 34(3):137–150, 1979.

[FPF07] I.M. Finn, N.J. Priebe, and D. Ferster. The emergence of contrast-invariant orientation tuning in simple cells of cat visual cortex. *Neuron*, 54(1):137–152, 2007.

[GLF+86] A. Grinvald, E. Lieke, R.D. Frostig, C.D. Gilbert, and T.N. Wiesel. Functional architecture of cortex revealed by optical imaging of intrinsic signals. *Nature*, 1986.

[GST03] M. Golubitsky, L.J. Shiau, and A. Török. Bifurcation on the visual cortex with weakly anisotropic lateral coupling. *SIAM Journal on Applied Dynamical Systems*, 2(2):97–143, 2003.

[HBH+03] Michael Heroux, Roscoe Bartlett, Vicki Howle Robert Hoekstra, Jonathan Hu, Tamara Kolda, Richard Lehoucq, Kevin Long, Roger Pawlowski, Eric Phipps, Andrew Salinger, Heidi Thornquist, Ray Tuminaro, James Willenbring, and Alan Williams. An Overview of Trilinos. Technical Report SAND2003-2927, Sandia National Laboratories, 2003.

[HBW03] A. Hutt, M. Bestehorn, and T. Wennekers. Pattern formation in intracortical neuronal fields. *Network: Computation in Neural Systems*, 14:351–368, 2003.

[HG91] Judith A Hirsch and Charles D Gilbert. Synaptic physiology of horizontal connections in the cat's visual cortex. *The Journal of Neuroscience*, 11(6):1800–1809, 1991.

[HG97] Chuanze Hou and Martin Golubitsky. An example of symmetry breaking to heteroclinic cycles. *journal of differential equations*, 133(1):30–48, 1997.

[Hoy06] R.B. Hoyle. *Pattern formation: an introduction to methods*. Cambridge Univ Pr, 2006.

[HW62] D.H. Hubel and T.N. Wiesel. Receptive fields, binocular interaction and functional architecture in the cat visual cortex. *J Physiol*, 160:106–154, 1962.

[HW77] D.H. Hubel and T.N. Wiesel. Functional architecture of macaque monkey. *Proceedings of the Royal Society, London [B]*, pages 1–59, 1977.

[KBT+03] T. Kenet, D. Bibitchkov, M. Tsodyks, A. Grinvald, and A. Arieli. Spontaneously emerging cortical representations of visual attributes. *Nature*, 425(6961):954–956, 2003.

[KLK+10] Min-Suk Kang, Sang-Hun Lee, June Kim, David Heeger, and Randolph Blake. Modulation of spatiotemporal dynamics of binocular rivalry by collinear facilitation and pattern-dependent adaptation. *Journal of vision*, 10(11):3, 2010.

[KSL+10] M. Kaschube, M. Schnabel, S. Löwel, D.M. Coppola, L.E. White, and F. Wolf. Universality in the evolution of orientation columns in the visual cortex. *Science*, 330(6007):1113, 2010.

[LAB03a] Jennifer S. Lund, Alessandra Angelucci, and Paul C. Bressloff. Anatomical substrates for functional columns in macaque monkey primary visual cortex. *Cerebral Cortex*, 12:15–24, 2003.

[LAB03b] J.S. Lund, A. Angelucci, and P.C. Bressloff. Anatomical substrates for functional columns in macaque monkey primary visual cortex. *Cerebral Cortex*, 13(1):15, 2003.

[LR92] Reiner Lauterbach and Mark Roberts. Heteroclinic cycles in dynamical systems with broken spherical symmetry. *Journal of differential equations*, 100(1):22–48, 1992.

[LS05] Huiyuan Li and Jiachang Sun. Fast fourier transform on hexagons. In *Current Trends in High Performance Computing and Its Applications*, pages 357–362. Springer, 2005.

[Mil72] W. Miller. *Symmetry groups and their applications*. Academic Press, 1972.

[MSL+05] J. Mariño, J. Schummers, D.C. Lyon, L. Schwabe, O. Beck, P. Wiesing, K. Obermayer, and M. Sur. Invariant computations in local cortical networks with balanced excitation and inhibition. *Nature neuroscience*, 8(2):194–201, 2005.

[PGS06] MJ Parker, M.G.M. Gomes, and IN Stewart. Forced symmetry-breaking of square lattice planforms. *Journal of Dynamics and Differential Equations*, 18(1):223–255, January 2006.

[RBH05] A. Roxin, N. Brunel, and D. Hansel. Role of Delays in Shaping Spatiotemporal Dynamics of Neuronal Activity in Large Networks. *Physical Review Letters*, 94(23):238103, 2005.

[Sch78] Doris Schattschneider. The plane symmetry groups: their recognition and notation. *American mathematical monthly*, pages 439–450, 1978.

[Tur52] A.M. Turing. The chemical basis of morphogenesis. *Philosophical Transactions of the Royal Society of London. Series B, Biological Sciences*, 237(641):37–72, 1952.

[Vel11] Romain Veltz. *Nonlinear analysis methods in neural field models*. PhD thesis, Université Paris Est, 2011.

[Vel13] Romain Veltz. Interplay between synaptic delays and propagation delays in neural fields equations. Rapport de recherche RR-8020, INRIA, January 2013.

[VF10] Romain Veltz and Olivier Faugeras. Local/global analysis of the stationary solutions of some neural field equations. *SIAM Journal on Applied Dynamical Systems*, 9(3):954–998, August 2010.

[WBL01] Hugh R Wilson, Randolph Blake, and Sang-Hun Lee. Dynamics of travelling waves in visual perception. *Nature*, 412(6850):907–910, 2001.

[WG98] F. Wolf and T. Geisel. Spontaneous pinwheel annihilation during visual development. *Nature*, 395(6697):73–78, 1998.

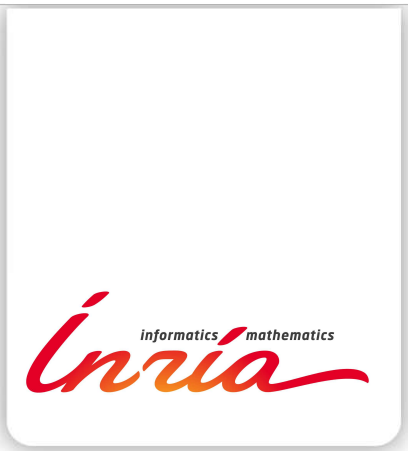

RESEARCH CENTRE
SOPHIA ANTIPOLIS – MÉDITERRANÉE

2004 route des Lucioles - BP 93
06902 Sophia Antipolis Cedex

Publisher
Inria
Domaine de Voluceau - Rocquencourt
BP 105 - 78153 Le Chesnay Cedex
inria.fr

ISSN 0249-6399